

Electronic Supporting Information (ESI):

Interplay between photo-, mechano- and thermo-chromism and single-ion-magnetism of two mononuclear dysprosium-anthracenephosphonate complexes

Xin-Da Huang,^a Mohamedally Kurmoo,^b Song-Song Bao,^a Kun Fan,^a Yan Xu,^a Zhao-Bo Hu,^a and Li-Min Zheng^{a*}

^aState Key Laboratory of Coordination Chemistry, School of Chemistry and Chemical Engineering, Collaborative Innovation Center of Advanced Microstructures, Nanjing University, Nanjing 210023, P. R. China.

^bInstitue de Chimie de Strasbourg, CNRS-UMR7177, Université de Strasbourg, 4 rue Blaise Pascal, Strasbourg Cedex 67007, France.

E-mail: lmzheng@nju.edu.cn

Experimental Section

Materials and measurements. The ligand 9-diethyl-phosphonomethylanthracene (depma) was synthesized according to the literature.¹ All the other starting materials were of analytical grade obtained from commercial sources and used without further purification. Elemental analyses for C, H and N were carried out on a PE 240C analyzer. Powder X-ray diffraction (PXRD) data were collected on a Bruker D8 advance diffractometer using Cu-K α radiation in a range of 5-50°. Single crystal diffraction data were collected at 123 K on Bruker D8 Venture or Smart Apex duo diffractometers at room temperature. The ac and dc magnetization data were obtained on polycrystalline samples using Quantum Design VSM and MPMS-XL7 SQUID magnetometers. The UV/Vis spectra were measured on a Perkin Elmer Lambda 950 UV/VIS/NIR spectrometer using powder samples. The infrared spectra were recorded on a Bruker Tensor 27 spectrometer in 600-4000 cm⁻¹ region. Thermogravimetric analyses were performed on a Mettler Toledo TGA/DSC 1 instrument in the range of 30-500 °C under a nitrogen flow (20 mL/min) at a heating rate of 10 °C min⁻¹. The steady fluorescence spectra were obtained at Bruker Spectrofluorometer LS55. Time-resolved fluorescence measurements were carried out on a Fluorolog TCSPC spectrofluorometer (Horiba Scientific) equipped with laser exciting at 370 nm.

Synthesis of [Dy(depma)₃(NO₃)₃] (1). A CH₃OH (10 mL) solution of Dy(NO₃)₃·6H₂O (0.1 mmol, 45.6 mg) and depma (0.3 mmol, 98.5 mg) was stirred at room temperature for 6 h and was then filtered and left at room temperature for several days to afford yellow block crystals with a yield of 66%. Elemental anal. Calcd (%): C, 51.29; H, 4.72; N, 3.15. Found (%): C, 51.83; H, 4.88; N, 3.04. IR (cm⁻¹): 3048(vw), 2986(w), 2938(w), 2905(w), 1623(w), 1491(s), 1414(w), 1387(w), 1301(s), 1249(m), 1166(vs), 1100(vw), 1054(s), 1032(s), 965(m), 891(m), 814(w), 782(m), 735(m), 690(w), 649(w).

Synthesis of [Dy(depma)₄(NO₃)₂(CF₃SO₃)] (2). After stirring a methanol solution containing Dy(CF₃SO₃)₃ (0.1 mmol, 61.0 mg), NH₄NO₃ (0.2 mmol, 16.1 mg), and depma (0.4 mmol, 131.0 mg) for 6 h, it was filtered and evaporated slowly in air at room temperature for 5 days to give faint yellow block crystals; yield = 50.2 mg (28.7 %). Elemental anal. Calcd (%): C, 52.88; H, 4.84; N, 1.60. Found (%): C, 52.89; H, 4.96; N, 1.49. IR (cm⁻¹): 3052(w), 2986(m), 2938(vw), 2906(w), 1623(w), 1509(s), 1447(w), 1417(w), 1389(w), 1301(s), 1247(s), 1173(vs), 1037(vs), 977(m), 890(m), 848(vw), 820(m), 784(m), 738(s), 692(w), 635(m).

Reference:

- 1 D. K. Cao, Y. W. Gu, J. Q. Feng, Z. S. Cai and M. D. Ward, *Dalton Trans.*, 2013, **42**, 11436.

Table S1. Crystallographic data for **1**, **2** and depma.

	1	2	depma
Empirical formula	C ₅₇ H ₆₃ N ₃ O ₁₈ P ₃ Dy	C ₇₇ H ₈₄ DyF ₃ N ₂ O ₂₁ P ₄ S	C ₁₉ H ₂₁ O ₃ P
Temperature (K)	123(2)	123(2)	150(2)
FW	1333.51	1748.90	328.33
Crystal system	Triclinic	Triclinic	Triclinic
Space group	<i>P</i> -1	<i>P</i> -1	<i>P</i> -1
a (Å)	11.5466(4)	14.011(1)	9.5176(7)
b (Å)	13.1727(5)	14.140(1)	9.6204(7)
c (Å)	21.0251(8)	20.115(2)	10.3715(7)
α (deg)	73.298(1)	77.771(1)	107.538(2)
β (deg)	88.041(1)	88.694(1)	97.061(2)
γ (deg)	71.072(1)	89.553(1)	108.815(2)
V (Å ³)	2891.2(2)	3893.6(6)	831.2(1)
Z	2	2	2
ρ _{calcd} (g cm ⁻³)	1.532	1.492	1.321
F(000)	1362	1794	348
goodness-of-fit on F ²	1.051	1.032	1.048
R1, wR2 [I > 2σ(I)] ^a	0.0355, 0.0791	0.0604, 0.1527	0.0462, 0.1213
R1 , wR2 (all data) ^a	0.0432, 0.0822	0.0754, 0.1635	0.0566, 0.1276
CCDC number	1815094	1815095	1815093

$$^a R_1 = \sum \| F_O \| - \| F_C \| / \sum \| F_O \|, \sigma R_2 = [\sum \sigma (F_O^2 - F_C^2)^2 / \sum \sigma (F_O^2)^2]^{1/2}$$

Table S2. Continuous Shape Measure (CShM) analyses of dysprosium geometries for **1** and **2** with 83% occupancy using the SHAPE2.1 Software.

Geometry	Complex 1	Complex 2
Enneagon (D_{9h})	33.334	33.846
Octagonal pyramid (C_{8v})	20.676	23.257
Heptagonal bipyramid (D_{7h})	16.036	18.589
Johnson triangular cupola J3 (C_{3v})	13.835	14.515
Capped cube J8 (C_{4v})	10.187	10.557
Spherical-relaxed capped cube	8.904	9.074
Capped square antiprism J10 (C_{4v})	3.057	2.593
Spherical capped square antiprism	2.135	1.217
Tricapped trigonal prism J51 (D_{3h})	3.402	2.685
Spherical tricapped trigonal prism	2.775	1.558
Tridiminished icosahedron J63	11.712	12.275
Hula-hoop (C_{2v})	10.288	11.789
Muffin (Cs)	2.301	1.167

Table S3. Selected bond lengths (\AA) and bond angles ($^\circ$) for **1** at 123 K.

Dy1-O1	2.3139(18)	O4-Dy1-O17	79.29(6)
Dy1-O4	2.3148(18)	O7-Dy1-O10	80.55(6)
Dy1-O7	2.3268(18)	O7-Dy1-O11	126.73(6)
Dy1-O10	2.435(2)	O7-Dy1-O13	71.91(6)
Dy1-O11	2.4752(17)	O7-Dy1-O14	123.39(7)
Dy1-O13	2.510(2)	O7-Dy1-O16	76.48(7)
Dy1-O14	2.4210(19)	O7-Dy1-O17	90.66(7)
Dy1-O16	2.503(2)	O10-Dy-O11	52.12(6)
Dy1-O17	2.444(2)	O10-Dy1-O13	71.21(6)
O1-Dy1-O4	86.85(6)	O10-Dy1-O14	76.96(7)
O1-Dy1-O7	78.18(6)	O10-Dy1-O16	153.90(7)
O1-Dy1-O10	85.80(6)	O10-Dy1-O17	141.70(7)
O1-Dy1-O11	75.70(6)	O11-Dy1-O13	107.70(6)
O1-Dy1-O13	144.62(6)	O11-Dy1-O14	73.02(6)
O1-Dy1-O14	148.64(6)	O11-Dy1-O16	138.75(6)
O1-Dy1-O16	77.56(7)	O11-Dy1-O17	141.06(7)
O1-Dy1-O17	128.98(6)	O13-Dy1-O14	51.78(6)
O4-Dy1-O7	150.67(6)	O13-Dy1-O16	112.31(6)
O4-Dy1-O10	123.72(6)	O13-Dy1-O17	70.62(6)
O4-Dy1-O11	72.01(6)	O14-Dy1-O16	126.51(7)
O4-Dy1-O13	128.20(6)	O14-Dy1-O17	77.23(7)
O4-Dy1-O14	81.45(6)	O16-Dy1-O17	51.48(7)
O4-Dy1-O16	75.73(6)		

Table S4. The parameters defining the $\pi\cdots\pi$ interactions for **1** and depma.

compound	$\pi\cdots\pi$	$d_{\text{plane-plane}} (\text{\AA})$	$d_{\text{center}\cdots\text{center}} (\text{\AA})$	$d_{\text{c}\cdots\text{c}} (\text{\AA})^a$
1	P1...P1	3.440	3.748	3.739
	P2...P2	3.458	4.969	4.969
depma	P1...P1	3.432	4.252	4.253

^a This means the intermolecular distance of carbon-carbon atoms at 9, 10- positions of anthracene moieties.

Table S5. The parameters of C-H···π interactions and H-bonding for **1**, **2** and depma.

compound	D-H···A	d _{D···A} (Å)	d _{H···A} (Å)	Angle _{D-H···A} (°)
1	C9-H9···π	3.706	2.813	158.6
	C30-H30···π	3.432	2.558	147.3
	C47-H47···O15	3.399	2.624	139.1
	C25-H25···O15	3.530	2.652	153.9
2	C31-H31···O12	3.285	2.384	158.2
	C11-H11A···π	3.502	2.559	171.8
	C22-H22A···π	3.520	2.571	176.3
	C37-H37A···π	3.605	2.652	176.8
depma	C56-H56A···π	3.560	2.655	178.8
	C21-H21A···O21	3.391	2.637	136.5
depma	C42-H42A···O15	3.622	2.683	170.0
	C9-H9A···O1	3.544	2.668	153.7

Table S6. Selected bond lengths (\AA) and bond angles ($^\circ$) for **2** with 83% occupancy at 123 K.

Dy1-O1	2.315(4)	O4-Dy1-O20	69.4(2)
Dy1-O4	2.339(4)	O7-Dy1-O10	139.9(2)
Dy1-O7	2.317(4)	O7-Dy1-O13	135.4(2)
Dy1-O10	2.379(4)	O7-Dy1-O16	83.2(2)
Dy1-O13	2.279(6)	O7-Dy1-O17	74.2(2)
Dy1-O16	2.472(6)	O7-Dy1-O19	123.3(2)
Dy1-O17	2.510(8)	O7-Dy1-O20	71.9(3)
Dy1-O19	2.496(5)	O10-Dy1-O13	78.3(2)
Dy1-O20	2.477(8)	O10-Dy1-O16	128.0(2)
O1-Dy1-O4	81.5(2)	O10-Dy1-O17	68.8(2)
O1-Dy1-O7	151.9(2)	O10-Dy1-O19	141.9(2)
O1-Dy1-O10	86.1(2)	O10-Dy1-O20	141.6(2)
O1-Dy1-O13	77.7(1)	O13-Dy1-O16	76.2(2)
O1-Dy1-O16	79.8(2)	O13-Dy1-O17	73.1(2)
O1-Dy1-O17	128.6(2)	O13-Dy1-O19	139.7(2)
O1-Dy1-O19	124.0(2)	O13-Dy1-O20	127.9(2)
O1-Dy1-O20	72.5(2)	O16-Dy1-O17	137.4(2)
O4-Dy1-O7	90.7(2)	O16-Dy1-O19	132.5(2)
O4-Dy1-O10	141.2(2)	O16-Dy1-O20	51.4(3)
O4-Dy1-O13	72.7(2)	O17-Dy1-O19	82.7(2)
O4-Dy1-O16	71.3(2)	O17-Dy1-O20	68.9(2)
O4-Dy1-O17	69.4(2)	O19-Dy1-O20	70.5(2)
O4-Dy1-O19	139.9(2)	O4-Dy1-O20	99.5(3)

Table S7. Selected bond lengths (\AA) and bond angles ($^{\circ}$) for depma at 150 K.

P1-O1	1.4639(16)	O1-P1-O2	114.03(9)
P1-O2	1.5763(19)	O1-P1-O3	114.01(9)
P1-O3	1.5741(16)	O1-P1-C1	117.79(8)
P1-C1	1.7935(17)	O2-P1-O3	106.12(9)
O2-C16	1.441(3)	O2-P1-C1	101.02(9)
O3-C18	1.429(3)	O3-P1-C1	102.21(9)
C1-C2	1.516(3)	P1-O2-C16	121.95(17)
C2-C3	1.414(3)	P1-O3-C18	123.19(16)
C2-C15	1.412(2)	P1-C1-C2	114.05(13)
C3-C4	1.430(3)	C1-C2-C3	120.52(15)
C3-C8	1.438(3)	C1-C2-C15	119.71(16)
C4-C5	1.365(3)	C3-C2-C15	119.77(16)
C5-C6	1.418(3)	C2-C3-C4	123.13(16)
C6-C7	1.354(3)	C2-C3-C8	119.54(16)
C7-C8	1.431(3)	C4-C3-C8	117.33(16)
C8-C9	1.391(3)	C3-C4-C5	121.23(17)
C9-C10	1.394(3)	C4-C5-C6	121.21(18)
C10-C11	1.430(3)	C5-C6-C7	119.53(18)
C10-C15	1.435(3)	C6-C7-C8	121.49(18)
C11-C12	1.355(3)	C3-C8-C7	119.18(16)
C12-C13	1.413(3)	C3-C8-C9	119.98(17)
C13-C14	1.367(3)	C7-C8-C9	120.83(17)
C14-C15	1.434(3)	C8-C9-C10	120.99(17)
C16-C17	1.471(3)	C9-C10-C11	120.34(17)
C18-C19	1.448(4)	C9-C10-C15	119.85(16)

Table S8. The emission lifetimes at room temperature for depma, **1** and **2** excited at 370 nm.

compound	condition	$\lambda_{\text{em}}/\text{nm}$	τ_1/ns	τ_2/ns	τ_3	τ_{average}	χ^2
depma	solid	514	14.2 (69.5 %)	27.1 (30.5 %)		16.6	1.18
	ethanol solution	414	5.5			5.5	0.98
1	original	543	14.8 (42.2 %)	56.1 (57.8%)		25.8	1.20
	UV light irradiation at 365 nm	490	8.0(63.9 %)	3.4(25.1 %)	56.0(11.0 %)	6.4	1.17
		440	7.2 (72.1 %)	2.8 (27.9 %)			1.18
2		424	1.1 (64.8 %)	4.7 (35.2%)		1.5	1.18

Table S10. The fit parameters obtained from analyses of the ac susceptibilities of **1** under 1 kOe bias dc field.

T / K	$\chi_T / \text{cm}^3 \text{ mol}^{-1}$	$\chi_s / \text{cm}^3 \text{ mol}^{-1}$	$\ln(\tau / \text{s})$	α	R^2
1.9	6.05	0.21	-3.95	0.19	6.68×10^{-4}
2.0	5.72	0.20	-4.24	0.18	5.51×10^{-4}
2.2	5.27	0.19	-4.70	0.17	3.29×10^{-4}
2.4	4.76	0.19	-5.29	0.14	3.47×10^{-4}
2.6	4.47	0.18	-5.84	0.12	3.89×10^{-4}
2.8	4.17	0.16	-6.37	0.11	4.39×10^{-4}
3.0	3.94	0.18	-6.87	0.10	1.90×10^{-4}
3.2	3.73	0.18	-7.36	0.09	2.58×10^{-4}
3.4	3.52	0.17	-7.83	0.09	3.47×10^{-4}
3.6	3.33	0.21	-8.27	0.08	2.07×10^{-4}
3.8	3.18	0.21	-8.72	0.08	1.73×10^{-4}
4.0	3.05	0.18	-9.18	0.09	8.56×10^{-5}

Table S11. The fitting parameters obtained from analyses of the ac susceptibilities of **1** irradiated by UV light under 1 kOe bias dc field.

T / K	$\chi_T / \text{cm}^3 \text{ mol}^{-1}$	$\chi_s / \text{cm}^3 \text{ mol}^{-1}$	$\ln(\tau / \text{s})$	α	R^2
1.8	6.53	0.48	-3.89	0.17	1.03×10^{-4}
2.0	6.09	0.46	-4.29	0.17	1.48×10^{-4}
2.2	5.69	0.43	-4.63	0.17	1.16×10^{-4}
2.4	5.18	0.37	-5.17	0.17	1.25×10^{-3}
2.6	4.77	0.38	-5.73	0.13	5.18×10^{-4}
2.8	4.47	0.36	-6.27	0.12	3.22×10^{-4}
3.0	4.24	0.31	-6.76	0.13	3.44×10^{-4}
3.2	3.90	0.35	-7.27	0.10	1.42×10^{-4}
3.4	3.68	0.32	-7.73	0.11	3.63×10^{-4}
3.6	3.44	0.35	-8.20	0.09	2.27×10^{-4}
3.8	3.24	0.36	-8.63	0.09	1.81×10^{-4}
4.0	3.08	0.42	-9.01	0.08	3.21×10^{-4}

Table S12. The parameters obtained by fitting the ac magnetic susceptibilities of the ground and heated **1** under 1 kOe dc field.

T / K	$\chi_T / \text{cm}^3 \text{ mol}^{-1}$	$\chi_s / \text{cm}^3 \text{ mol}^{-1}$	$\ln(\tau / \text{s})$	α	R^2
1.8	5.15	0.56	-6.33	0.29	6.72×10^{-4}
2.0	4.75	0.62	-6.52	0.29	1.09×10^{-4}
2.2	4.38	0.61	-6.79	0.30	7.15×10^{-4}
2.4	4.07	0.63	-7.05	0.28	7.27×10^{-4}
2.6	3.77	0.66	-7.39	0.26	4.45×10^{-4}
2.8	3.50	0.61	-7.78	0.27	1.84×10^{-4}
3.0	3.35	0.73	-8.04	0.25	4.77×10^{-4}
3.2	3.15	0.63	-8.51	0.28	5.86×10^{-4}
3.4	2.96	0.71	-8.84	0.26	2.62×10^{-4}

Table S13. The fit parameters obtained from analyses of the ac susceptibilities of **2** under 0.5 kOe bias dc field.

T / K	$\chi_T/\text{cm}^3\text{mol}^{-1}$	$\chi_s/\text{cm}^3\text{mol}^{-1}$	$\ln(\tau / \text{s})$	α	R^2
1.8	5.48	0.42	-4.67	0.56	5.57×10^{-5}
2.0	5.35	0.45	-4.72	0.56	3.62×10^{-5}
2.2	5.09	0.50	-4.88	0.55	3.62×10^{-5}
2.4	4.75	0.54	-5.13	0.55	4.74×10^{-5}
2.6	4.47	0.59	-5.33	0.54	4.44×10^{-5}
2.8	4.24	0.62	-5.56	0.53	2.67×10^{-4}
3.0	4.01	0.63	-5.81	0.53	6.93×10^{-5}
3.2	3.79	0.66	-6.08	0.52	8.21×10^{-5}
3.4	3.56	0.68	-6.39	0.52	8.84×10^{-5}
3.6	3.36	0.73	-6.71	0.51	9.99×10^{-5}
3.9	3.08	0.87	-7.08	0.48	7.58×10^{-5}
4.2	2.86	0.91	-7.55	0.47	6.52×10^{-5}
4.5	2.66	0.97	-7.98	0.46	4.50×10^{-5}
4.8	2.49	1.08	-8.24	0.44	3.79×10^{-5}
5.1	2.34	1.14	-8.56	0.42	2.95×10^{-5}
5.4	2.21	1.20	-8.82	0.41	2.86×10^{-5}
5.7	2.10	1.25	-9.01	0.39	1.75×10^{-5}
6.0	2.00	1.28	-9.23	0.39	2.24×10^{-5}

Table S14. The fit parameters obtained from analyses of the ac susceptibilities of **2** under 1 kOe bias dc field.

T / K	$\chi_T / \text{cm}^3 \text{ mol}^{-1}$	$\chi_s / \text{cm}^3 \text{ mol}^{-1}$	$\ln(\tau / \text{s})$	α	R^2
1.8	5.19	0.21	-3.38	0.62	1.21×10^{-4}
2.0	4.90	0.32	-3.79	0.59	9.10×10^{-5}
2.2	4.71	0.38	-4.07	0.57	5.01×10^{-5}
2.4	4.49	0.44	-4.40	0.56	3.03×10^{-5}
2.6	4.28	0.48	-4.72	0.56	2.66×10^{-5}
2.8	4.08	0.52	-5.04	0.55	4.91×10^{-5}
3.0	3.87	0.57	-5.39	0.54	6.53×10^{-5}
3.2	3.67	0.61	-5.74	0.54	7.36×10^{-5}
3.4	3.48	0.66	-6.10	0.53	1.02×10^{-4}
3.6	3.30	0.71	-6.43	0.52	1.02×10^{-4}
3.8	3.08	0.80	-6.85	0.51	7.74×10^{-5}
4.2	2.89	0.86	-7.24	0.50	7.73×10^{-5}
4.5	2.71	0.95	-7.59	0.48	6.11×10^{-5}
4.8	2.58	0.97	-8.02	0.49	3.34×10^{-5}
5.1	2.41	1.06	-8.35	0.46	4.28×10^{-5}
5.4	2.28	1.14	-8.61	0.43	4.10×10^{-5}
5.7	2.15	1.20	-8.84	0.42	2.88×10^{-5}
6.0	2.04	1.25	-9.09	0.40	2.35×10^{-5}

Table S15. The fit parameters obtained from analyses of the ac susceptibilities for the ground **2** under 0.5 kOe bias dc field.

T / K	$\chi_T / \text{cm}^3 \text{mol}^{-1}$	$\chi_S / \text{cm}^3 \text{mol}^{-1}$	$\ln(\tau / \text{s})$	α	R^2
1.8	5.05	0.63	-6.95	0.60	2.73×10^{-5}
2.0	4.85	0.66	-6.98	0.60	3.42×10^{-5}
2.2	4.64	0.74	-6.98	0.59	2.97×10^{-5}
2.4	4.40	0.78	-7.03	0.58	4.00×10^{-5}
2.6	4.14	0.86	-7.05	0.57	3.36×10^{-5}
2.8	3.90	0.89	-7.14	0.56	3.37×10^{-5}
3.0	3.69	0.95	-7.17	0.56	3.34×10^{-5}
3.2	3.45	1.00	-7.33	0.54	3.43×10^{-5}
3.4	3.25	1.00	-7.52	0.54	3.84×10^{-5}
3.6	3.07	1.06	-7.63	0.52	4.10×10^{-5}
3.9	2.84	1.10	-7.86	0.50	4.01×10^{-5}
4.2	2.64	1.16	-8.05	0.48	3.98×10^{-5}
4.5	2.46	1.21	-8.23	0.47	3.25×10^{-5}
4.8	2.31	1.25	-8.40	0.45	2.71×10^{-5}

Table S16. The fit parameters obtained from analyses of the ac susceptibilities for the ground and heated **2** under 0.5 kOe bias dc field.

T / K	$\chi_T / \text{cm}^3 \text{mol}^{-1}$	$\chi_S / \text{cm}^3 \text{mol}^{-1}$	$\ln(\tau / \text{s})$	α	R^2
1.8	5.64	0.33	-6.50	0.62	5.31×10^{-5}
2.0	5.29	0.52	-6.48	0.60	3.78×10^{-5}
2.2	4.97	0.61	-6.54	0.59	6.31×10^{-5}
2.4	4.59	0.72	-6.62	0.57	5.84×10^{-5}
2.6	4.31	0.77	-6.73	0.57	6.46×10^{-5}
2.8	4.06	0.82	-6.84	0.56	7.53×10^{-5}
3.0	3.81	0.89	-6.93	0.55	7.18×10^{-5}
3.2	3.58	0.90	-7.10	0.54	8.10×10^{-5}
3.4	3.36	0.99	-7.21	0.52	7.98×10^{-5}
3.6	3.18	0.97	-7.47	0.52	1.15×10^{-4}
3.9	2.93	0.99	-7.80	0.50	7.58×10^{-5}
4.2	2.72	1.02	-8.15	0.49	6.56×10^{-5}
4.5	2.53	1.09	-8.41	0.47	4.51×10^{-5}
4.8	2.38	1.20	-8.47	0.44	6.93×10^{-5}

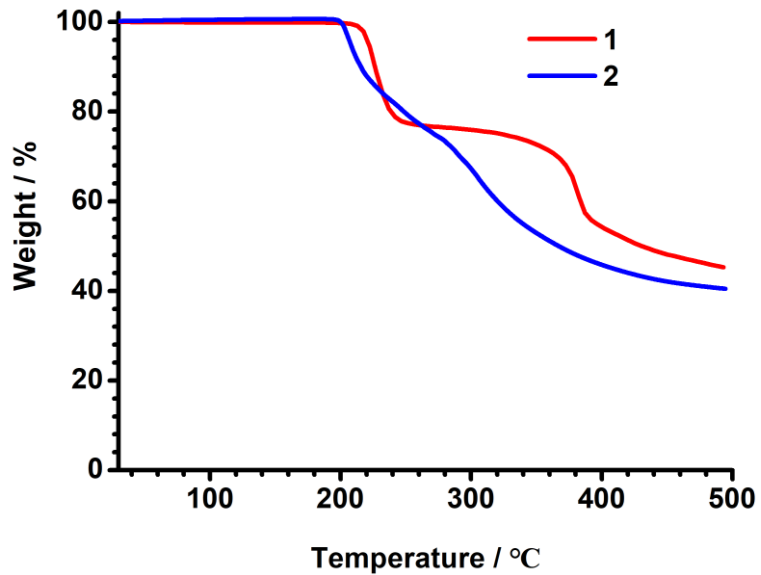


Figure S1. Thermogravimetric analyses of **1** (red) and **2** (blue) measured under nitrogen atmosphere at a heating rate of 10 °C/min.

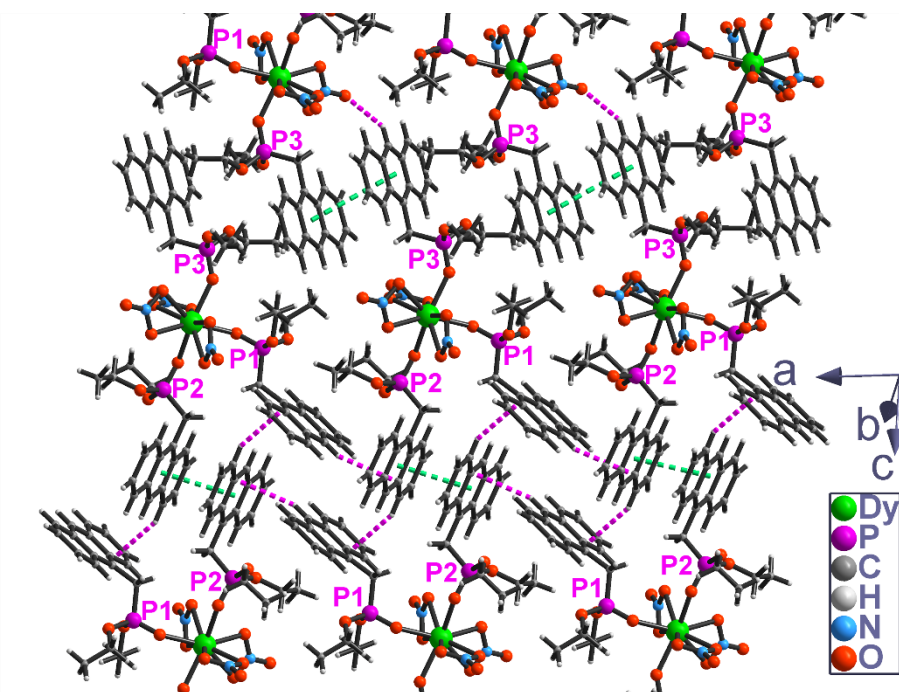


Figure S2. The $\pi\cdots\pi$ and $\text{C}-\text{H}\cdots\pi$ interactions, and H-bonds within the supramolecular layer in the structure of **1**.

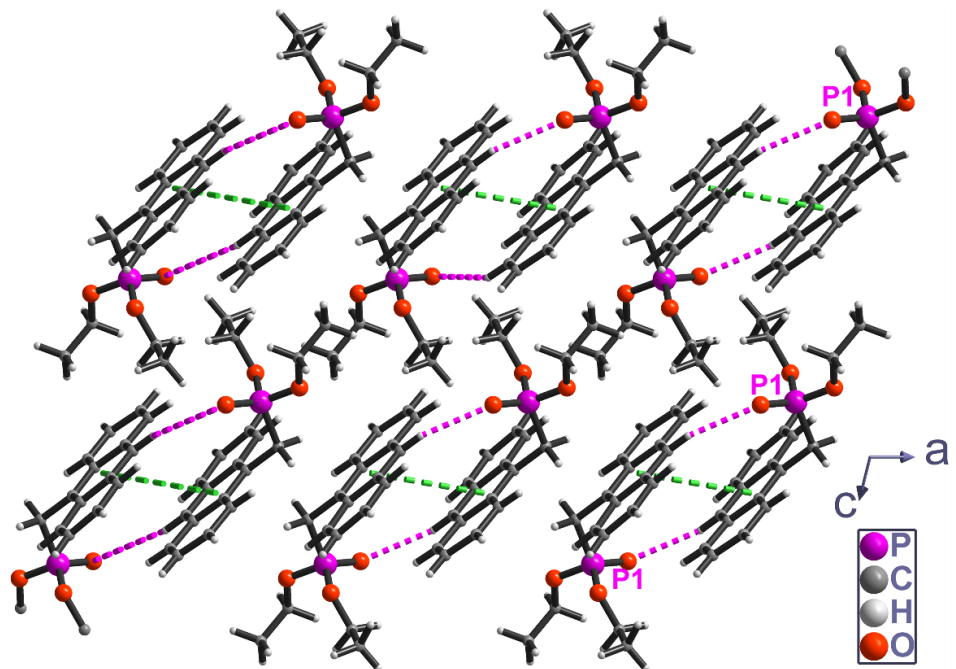


Figure S3. The structure of depma showing the $\pi\cdots\pi$ interactions (dotted green lines) and C-H...O hydrogen bond interactions (dotted purple lines).

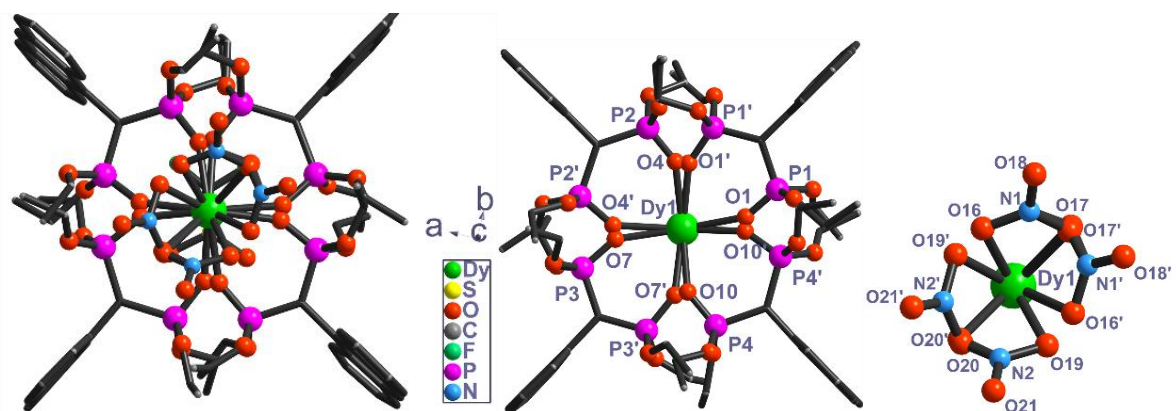


Figure S4. The structure of **2** showing both of the disordered parts.

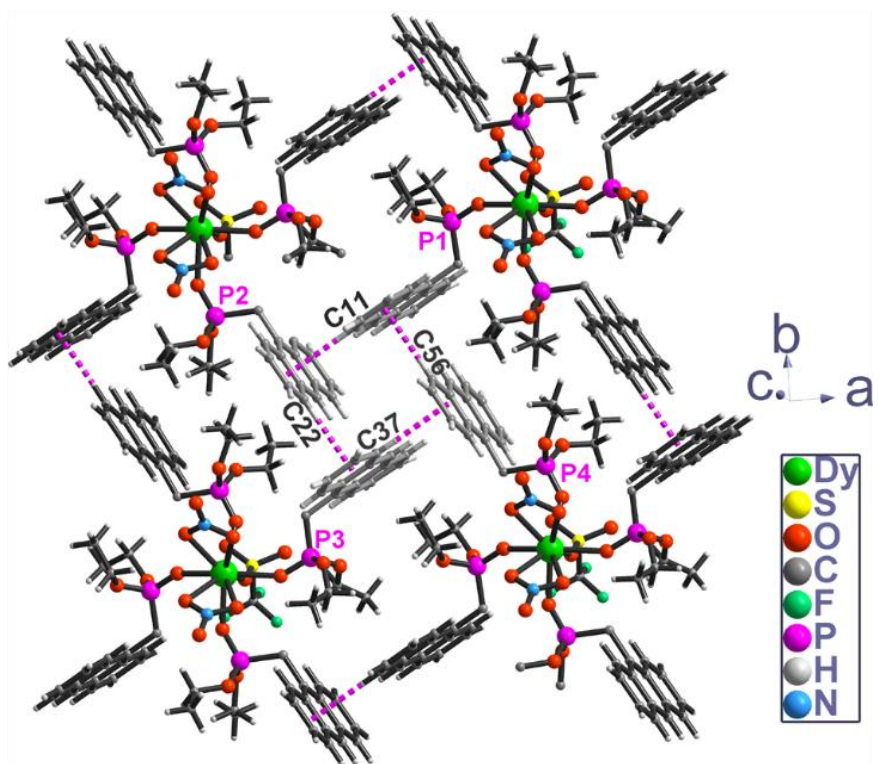


Figure S5. The C-H \cdots π interactions in the structure of **2**.

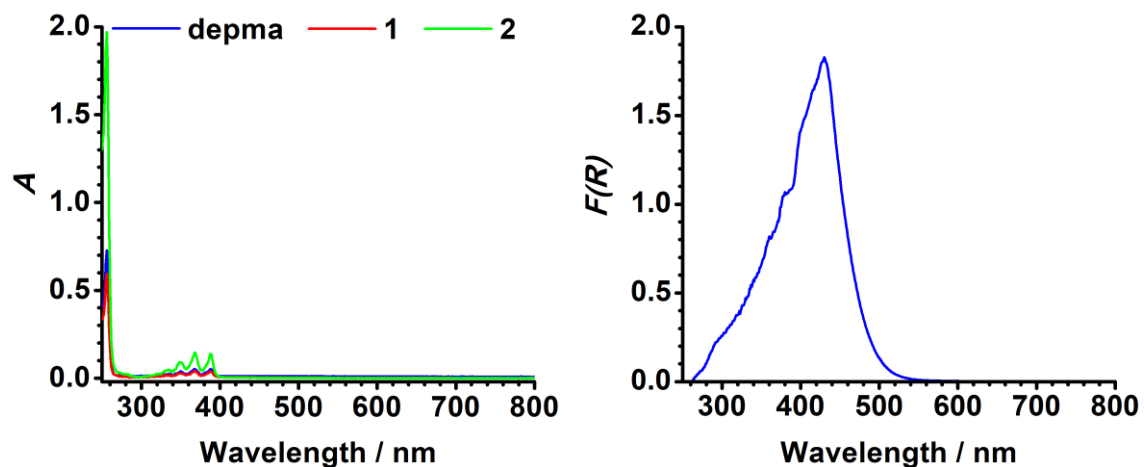


Figure S6. (Left) The UV-vis absorption spectra for ethanol solutions of the ligand depma (5×10^{-6} mol/L), and compounds **1** and **2** (1×10^{-6} mol/L). (Right) The UV-vis absorption spectra translated from the diffuse reflectance spectra using Kubelka-Munk function ($F(R) = (1 - R)^2/2R$) for the ligand depma.

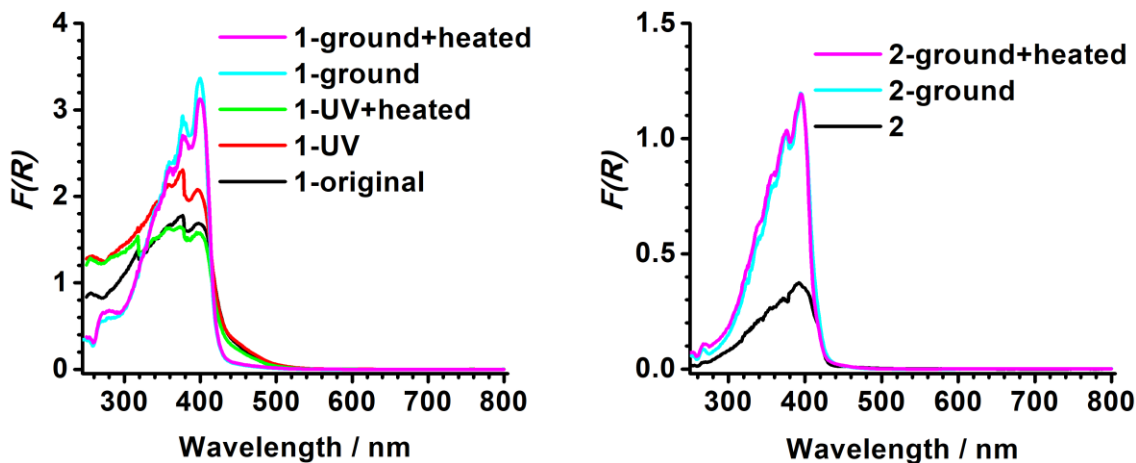


Figure S7. The UV-vis absorption spectra translated from the diffuse reflectance spectra using Kubelka-Munk function ($F(R) = (1 - R)^2/2R$) for compound **1** (left) and **2** (right) under different conditions. The black curves represent the original sample. The red and green curves represent the samples exposed to 365 nm UV light for 10 minutes and exposed sample heated 100°C for 10 min. The cyan curves represent the ground sample while the violet curves represent the ground samples that are heated at 100 °C for 2 hours.

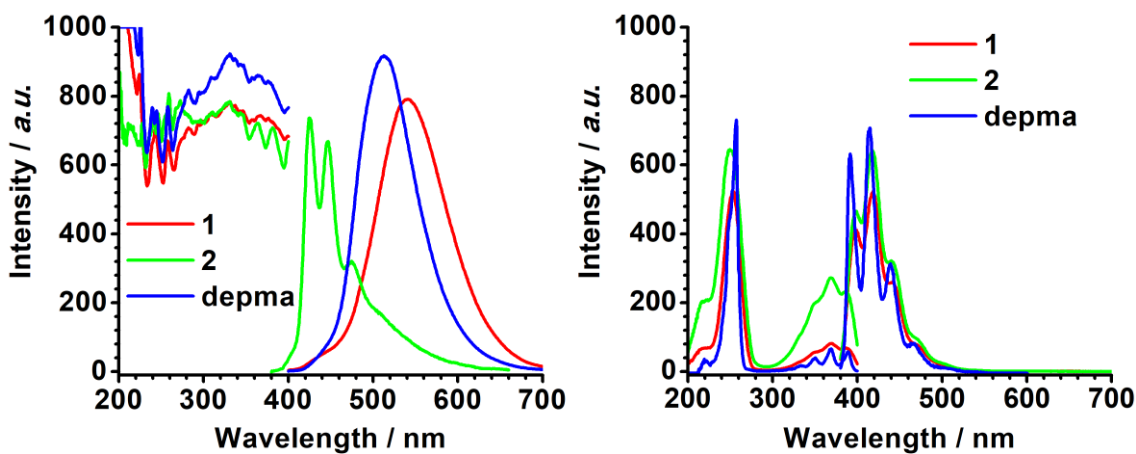


Figure S8. Left: Steady state excitation (with emission at 417 nm, 512 nm and 540 nm) and emission spectra excited at 330 nm for the powders of **1**, **2** and depma. Right: Steady state excitation with emission at 417 nm and emission spectra excited at 252 nm for the ethanol solution (1×10^{-6} mol/L) of **1**, **2** and depma.

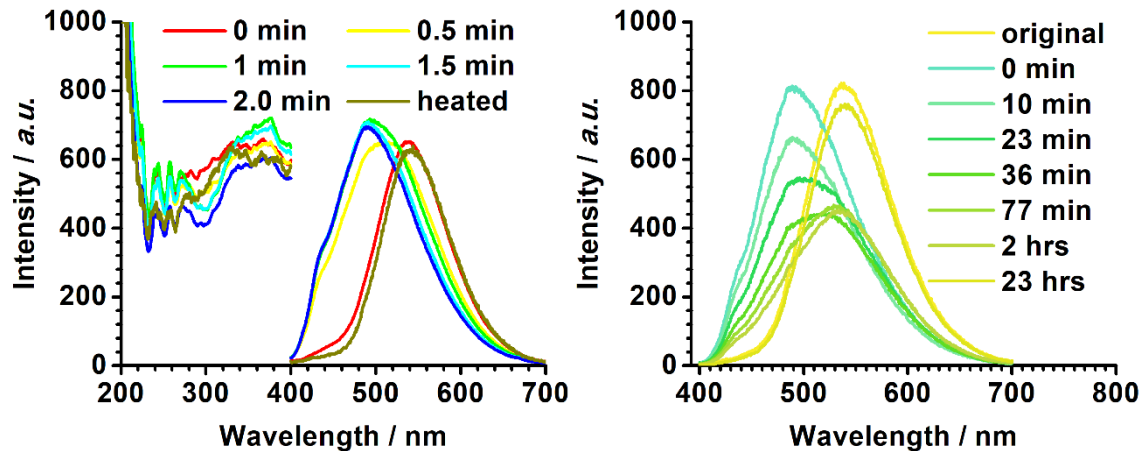


Figure S9. (Left) Excitation and emission spectra for compound **1** exposed to 365 nm UV light for different times. (Right) Emission spectra for compound **1** irradiated by UV light and then retained in the dark.

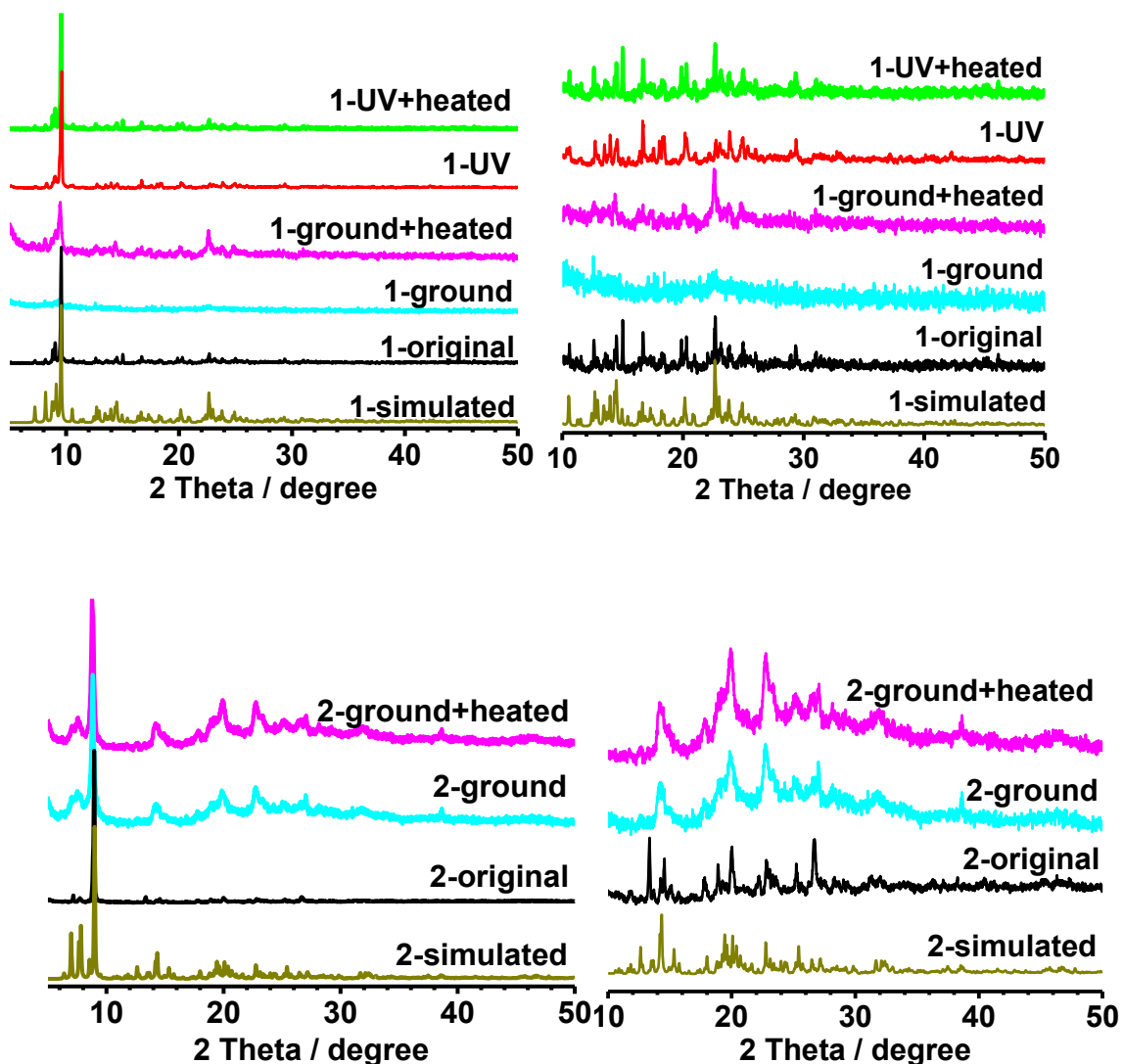


Figure S10. The PXRD patterns for compound **1** (top) and **2** (down) under different conditions. The red and green curves represent the samples exposed to 365 nm UV light for 10 minutes and the exposed sample kept at room temperature for 23 hours. The cyan curves represent the ground sample while the violet curves represent the ground sample that are heated at 100 °C for 2 hours.

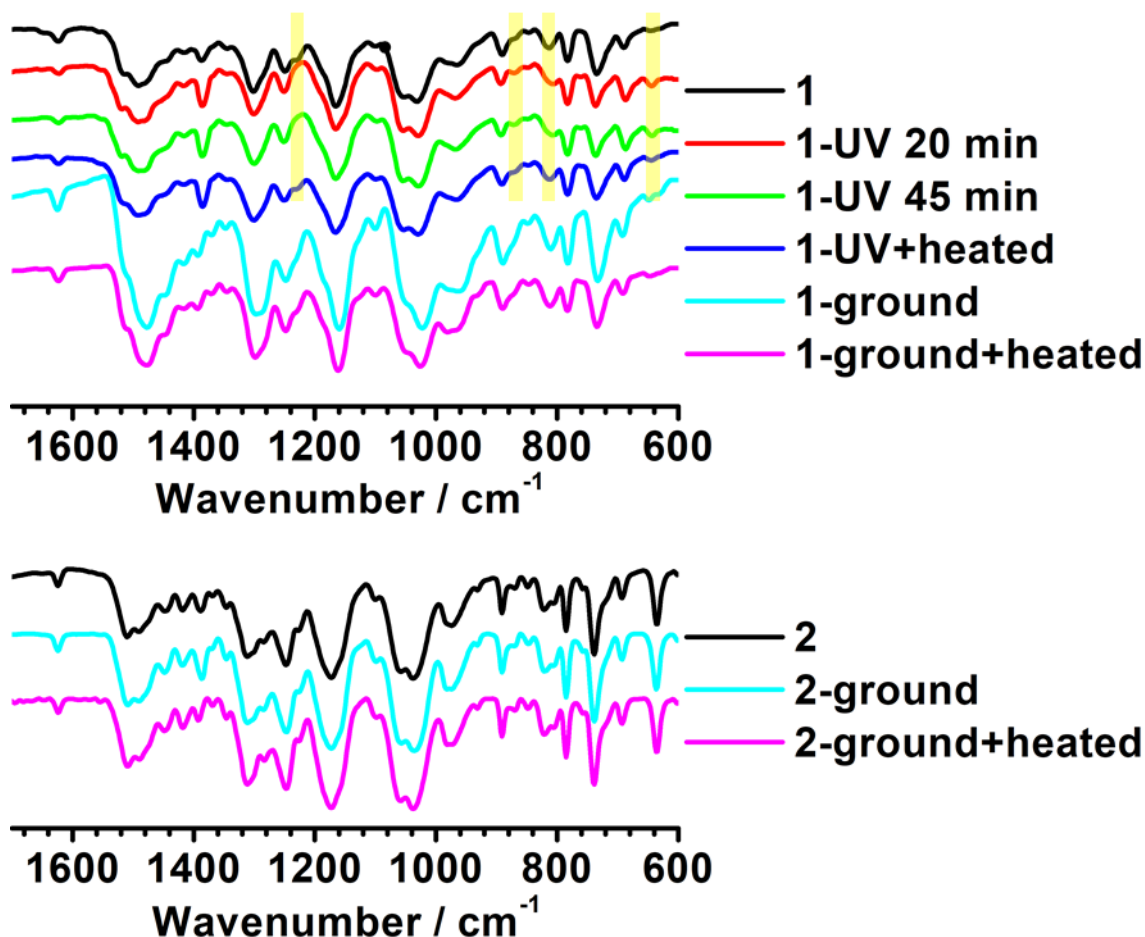


Figure S11. The FTIR spectra for **1** (a) and **2** (b) under different conditions. The black, red, green, and blue spectra were measured by using an ATR accessory while the others were obtained from the KBr pellets. The yellow highlight shows the changes possibly caused by photodimerization. The red and green curves represent the samples exposed to 365 nm UV light for 10 minutes and exposed sample heated at room temperature for 23 hours. The cyan curves represent the ground sample while the violet curves represent the ground samples that are heated at 100 °C for 2 hours.

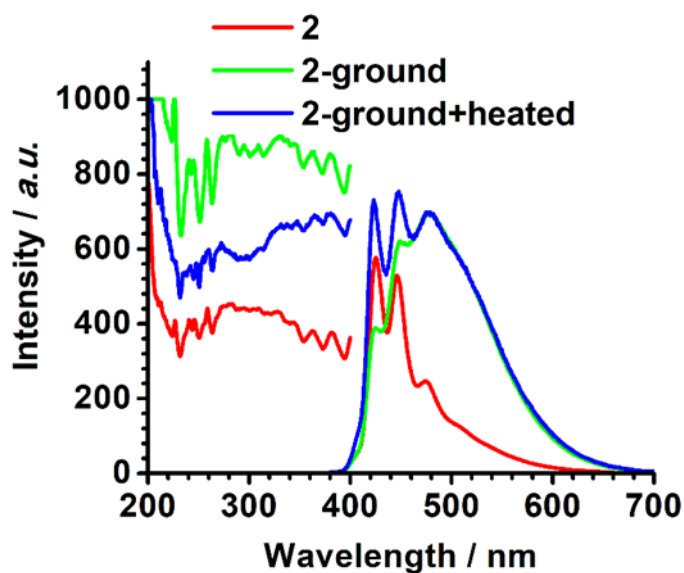


Figure S12. Excitation and emission spectra excited at 480 nm and 330 nm respectively for **2** (a), ground **2** (b), ground and heated **2** (c). The heating process was performed at 100 °C for 12 hours.

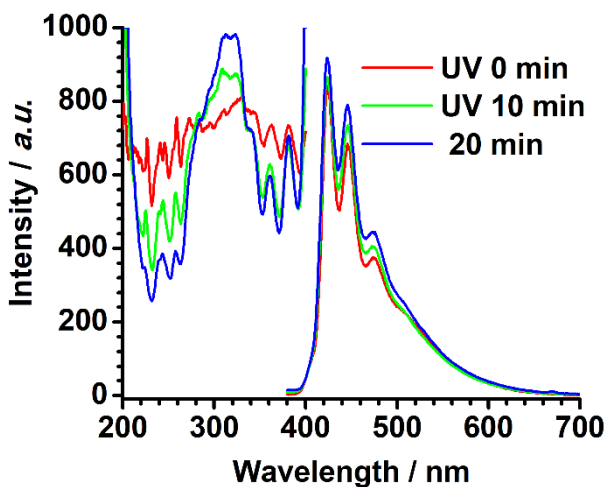


Figure S13. Excitation and emission spectra excited at 423 nm and 330 nm respectively for irradiated compound **2** by 365 nm UV light. There is no evident change of emission but large difference of the excitation spectra.

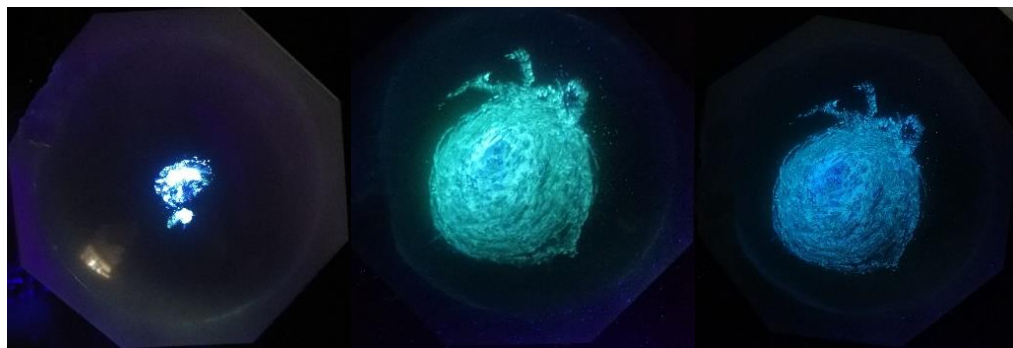


Figure S14. The pictures illustrate a pristine sample of **2** (left), ground **2** (middle) and then heated for 12 h (right).

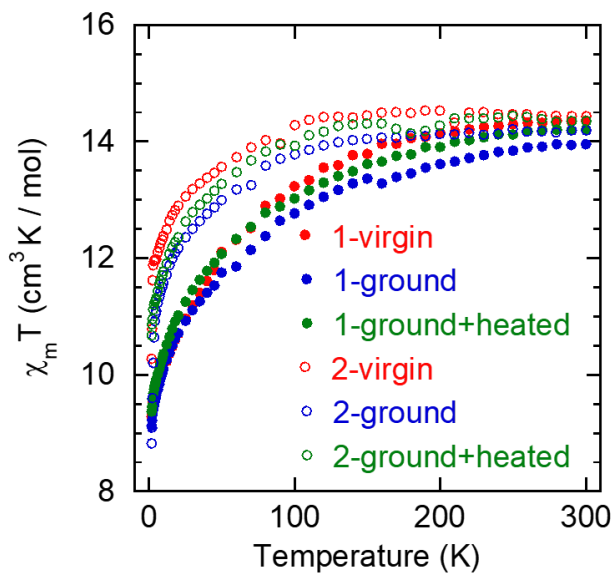


Figure S15. Temperature dependence of $\chi_m T$ on cooling in a field of 1 kOe for **1** (solid symbols) and **2** (open symbols). The red, blue and green symbols represent data for virgin, ground, and ground+heated samples. The $\chi_m T$ products at room temperature are 14.36, 13.95, 14.21, 14.43, 14.05 and 14.35 $\text{cm}^3 \text{K mol}^{-1}$ for **1**-virgin, **1**-ground, **1**-ground+heated, **2**-virgin, **2**-ground and **2**-ground+heated.

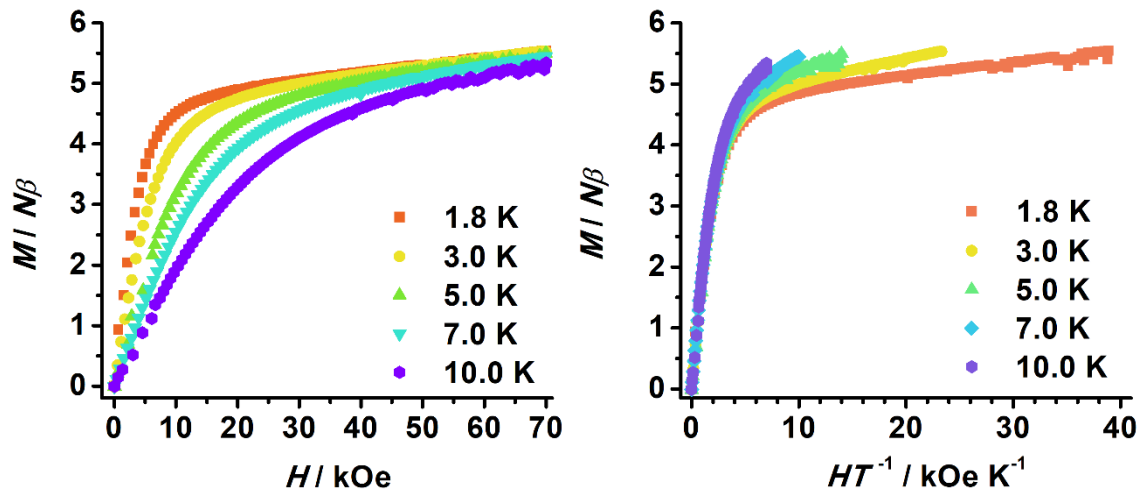


Figure S16. Field dependence of the magnetization (left) and the plot of magnetization M versus H/T (right) at depicted temperatures for compound 1.

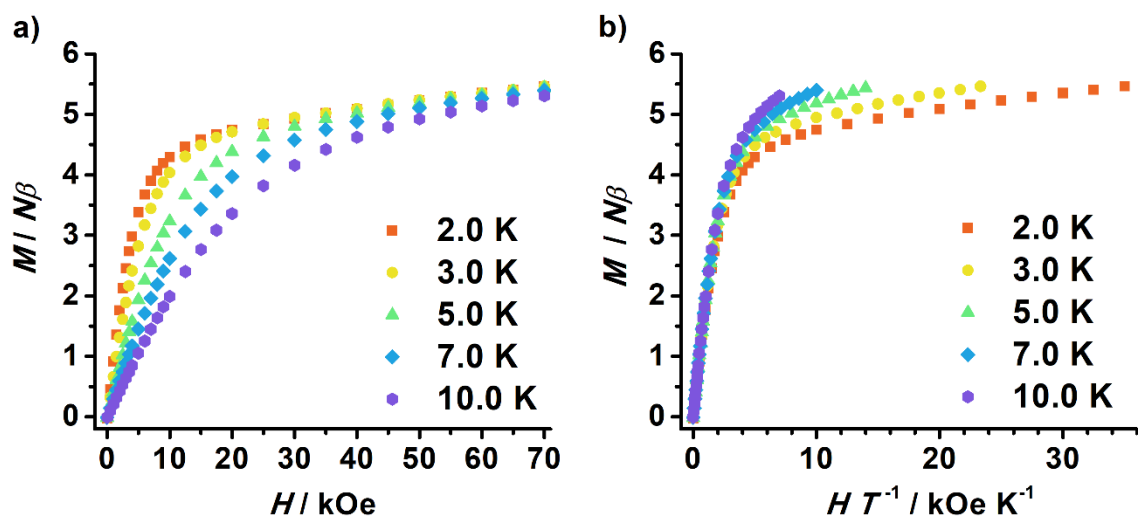


Figure S17. Field dependence of the magnetization (a) and isothermal magnetization M versus H/T (b) at depicted temperatures for compound 2.

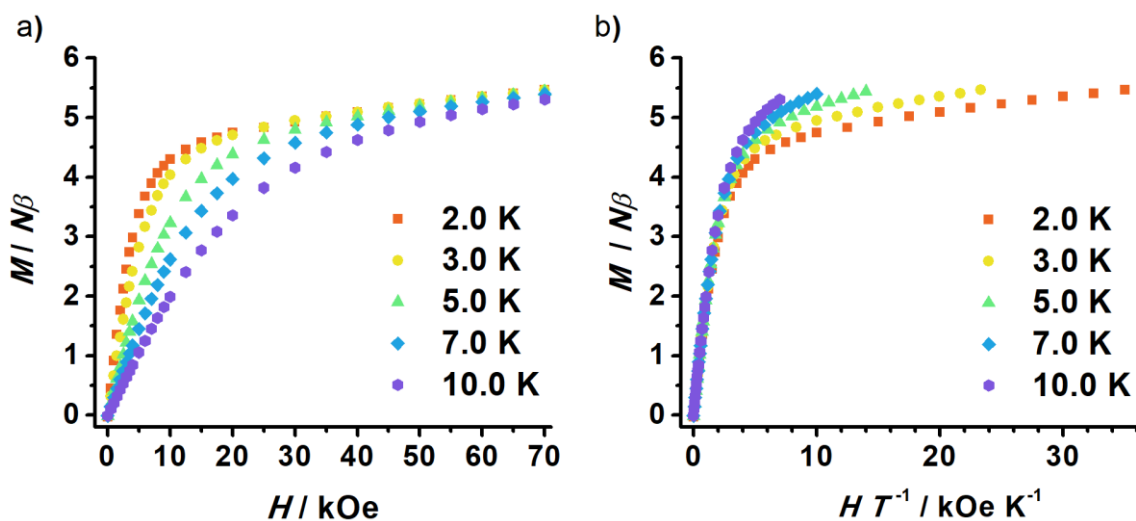


Figure S18. Field dependence of the magnetization and the plot of magnetization M versus H/T at depicted temperatures for ground and heated **1**.

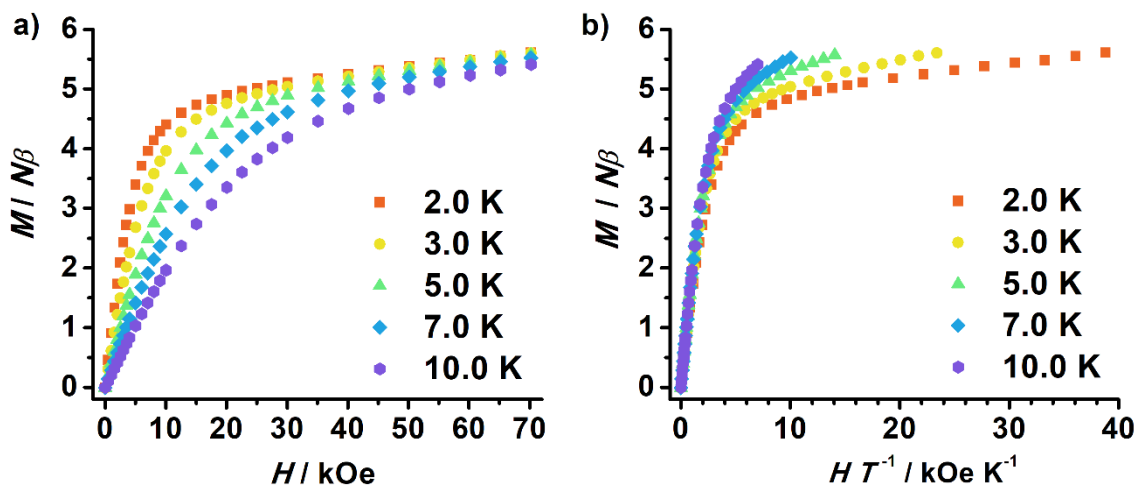


Figure S19. Field dependence of the magnetization and isothermal magnetization M versus H/T for ground **2** at depicted temperatures.

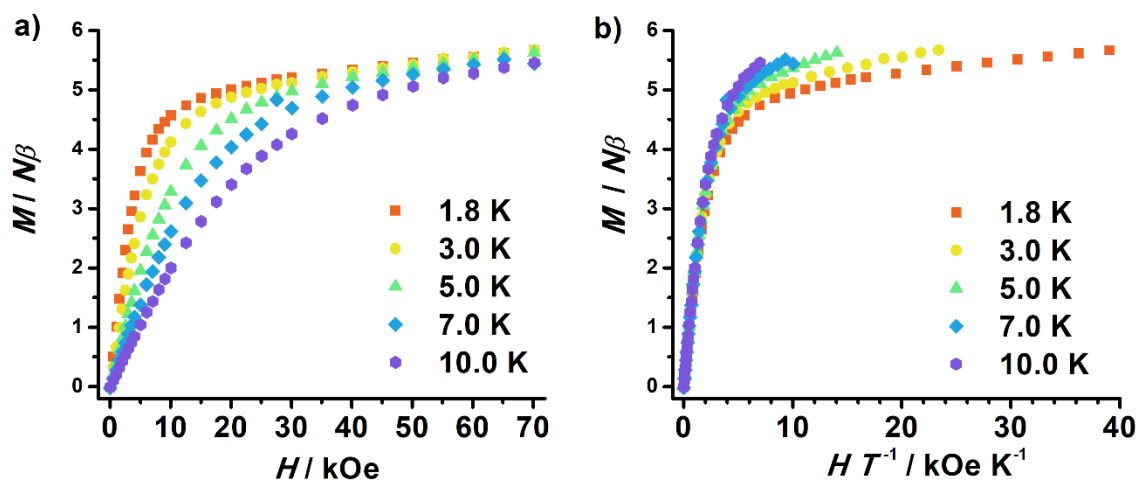


Figure S20. Field dependence of the magnetization and isothermal magnetization M versus H/T for ground and heated **2** at depicted temperatures.

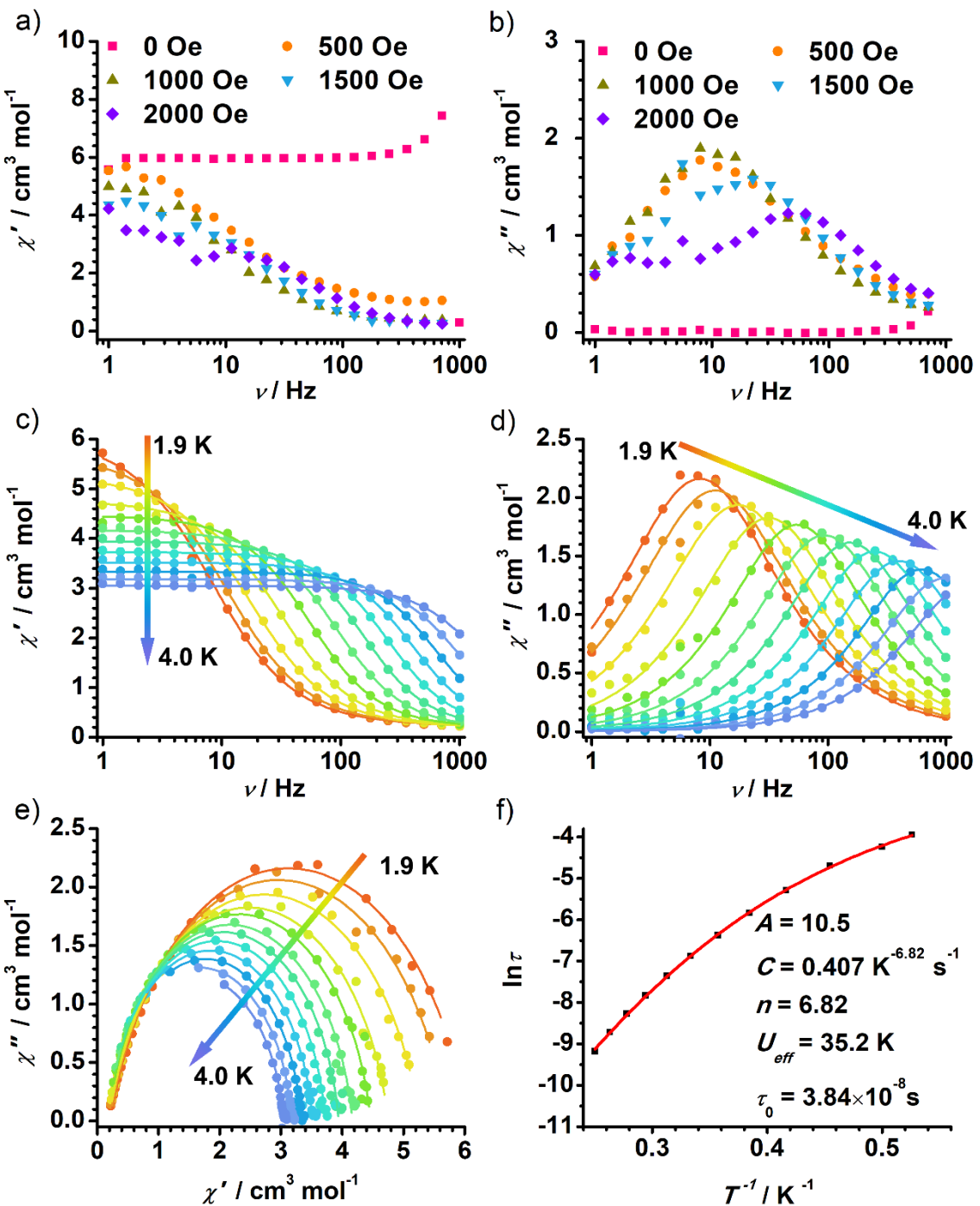


Figure S21. Frequency dependence of the in-phase (a) and out-of-phase (b) signals for **1** in the indicated dc fields at 1.8 K. Frequency dependence of the in-phase (χ' , c) and out of phase (χ'' , d) ac susceptibilities, Cole-Cole plots (e) and corresponding plot of $\ln \tau$ vs. T^{-1} (f) for **1**, measured in the temperature range 1.9–4.0 K under 1 kOe dc field. The solid line represents the best fitting.

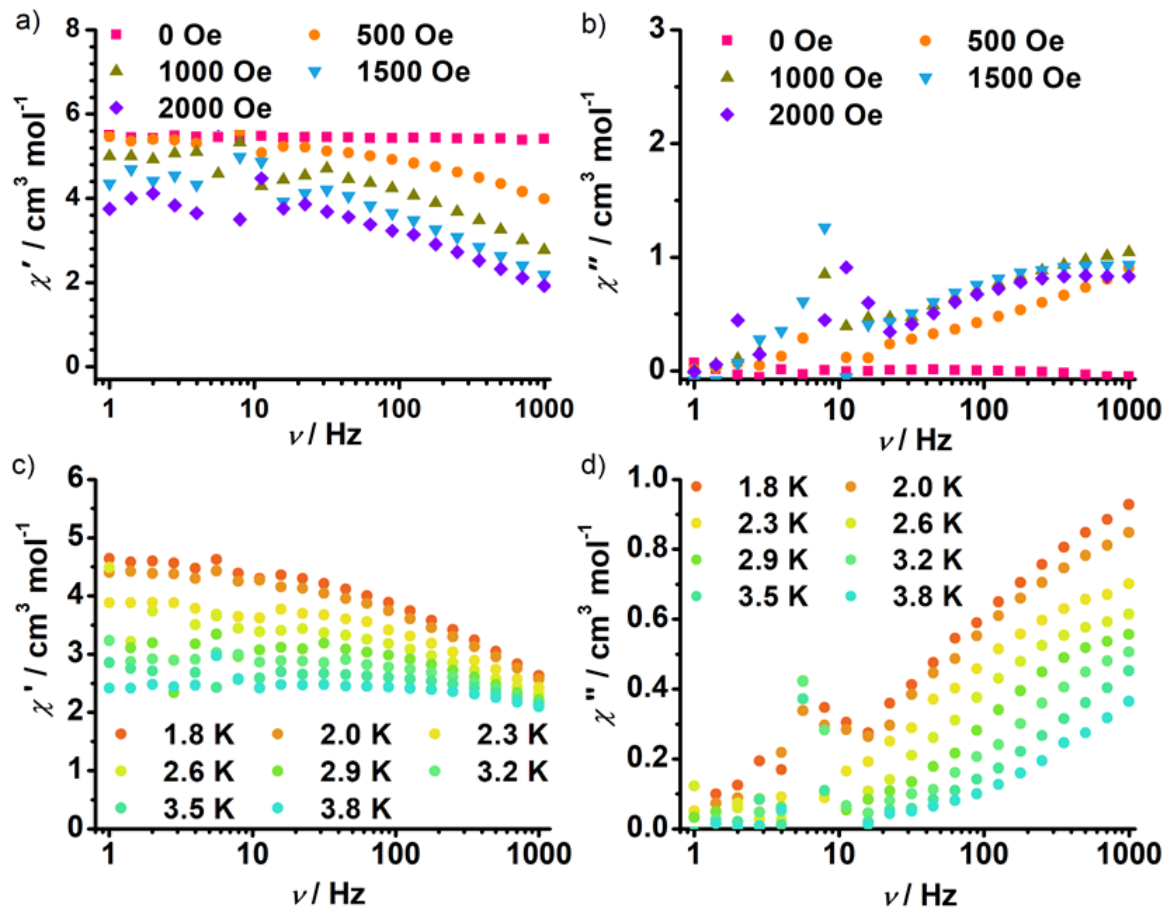


Figure S22. Frequency dependence of in-phase (χ' , a) and out-of-phase (χ'' , b) signals of **1** after grinding in the indicated dc fields at 1.8 K. Frequency dependence of the in-phase (χ' , c) and out-of-phase (χ'' , d) ac susceptibilities for **1** after grinding measured in the temperature range 1.8 – 3.8 K in a 1 kOe dc field.

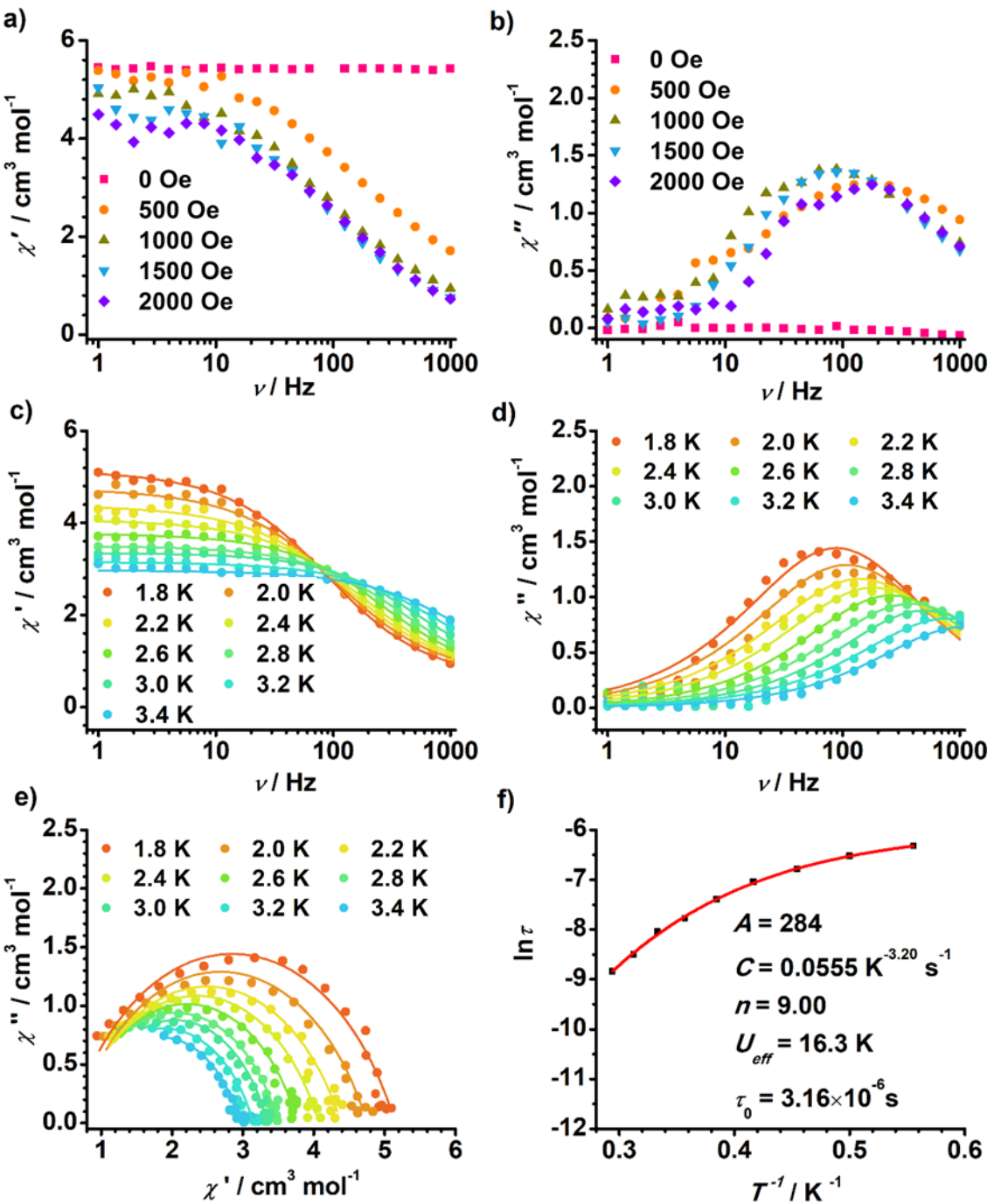


Figure S23. Frequency dependence of the in-phase (a) and out-of-phase (b) signals for ground and heated **1** in the indicated dc fields at 1.8 K. Frequency dependence of the in-phase (χ' , c) and out of phase (χ'' , d) ac susceptibilities, Cole-Cole plots (e) and corresponding plot of $\ln \tau$ vs. T^{-1} (f) for ground and heated **1**, measured in the temperature range 1.8–4.0 K under 1 kOe dc field. The solid line represents the best fitting.

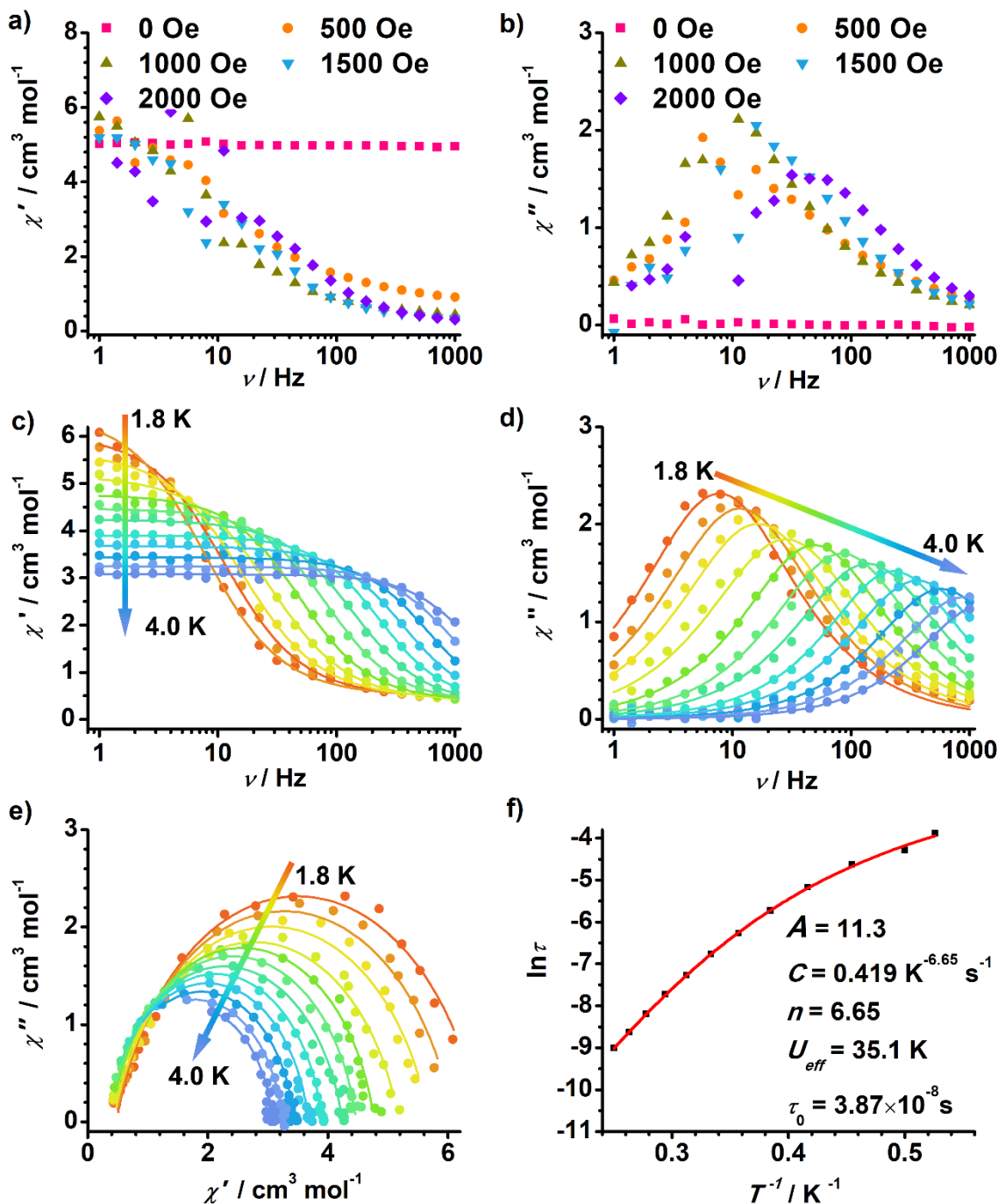


Figure S24. Frequency dependence of the in-phase (a) and out-of-phase (b) signals for compound **1** irradiated by 365 nm UV light in the indicated dc fields at 1.8 K. Frequency dependence of the in-phase (χ' , c) and out of phase (χ'' , d) ac susceptibility, Cole-Cole plots (e) and corresponding plot of $\ln \tau$ vs. T^{-1} (f) for compound **1** irradiated by 365 nm UV light for 3 hours, measured at 1 kOe dc field. The solid line represents the best fitting.

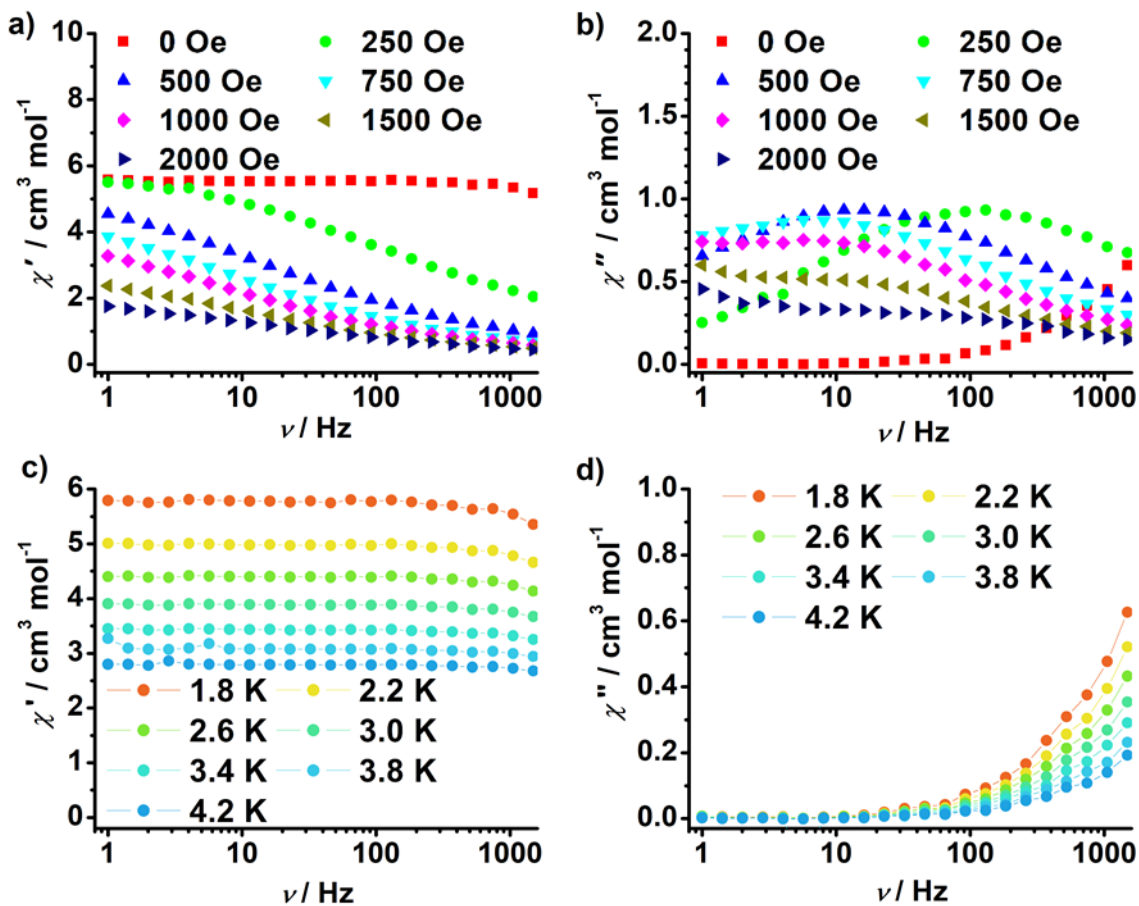


Figure S25. Frequency dependence of the in-phase (a) and out-of-phase (b) signals for compound **2** in the indicated dc fields at 1.8 K. Frequency dependence of the in-phase (c) and out-of-phase (d) signals for compound **2** under zero dc field.

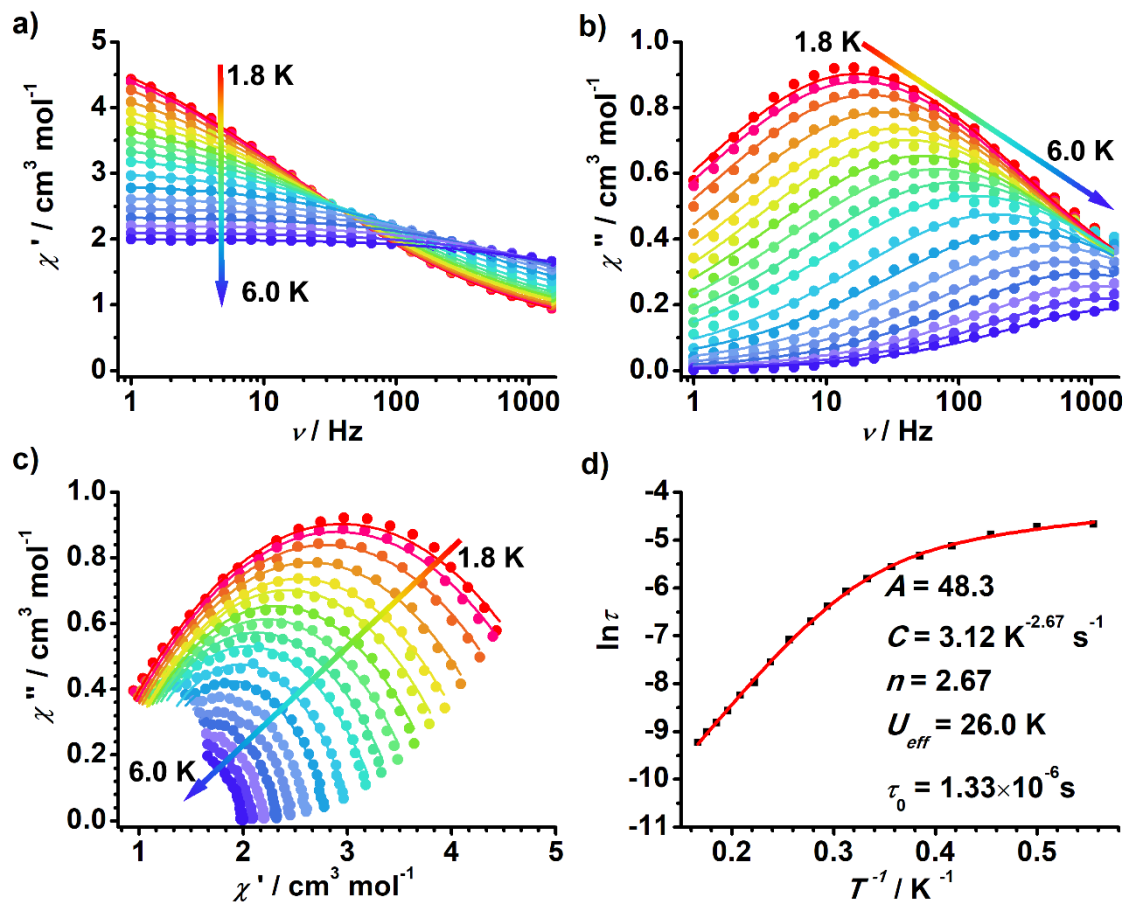


Figure S26. Frequency dependence of the in-phase (χ' , a) and out of phase (χ'' , b) ac susceptibilities, Cole-Cole plots (c) and corresponding plot of $\ln \tau$ vs. T^{-1} (d) for compound **2** measured at 0.5 kOe dc field between 1.8 K and 6.0 K. The solid line represents the best fitting.

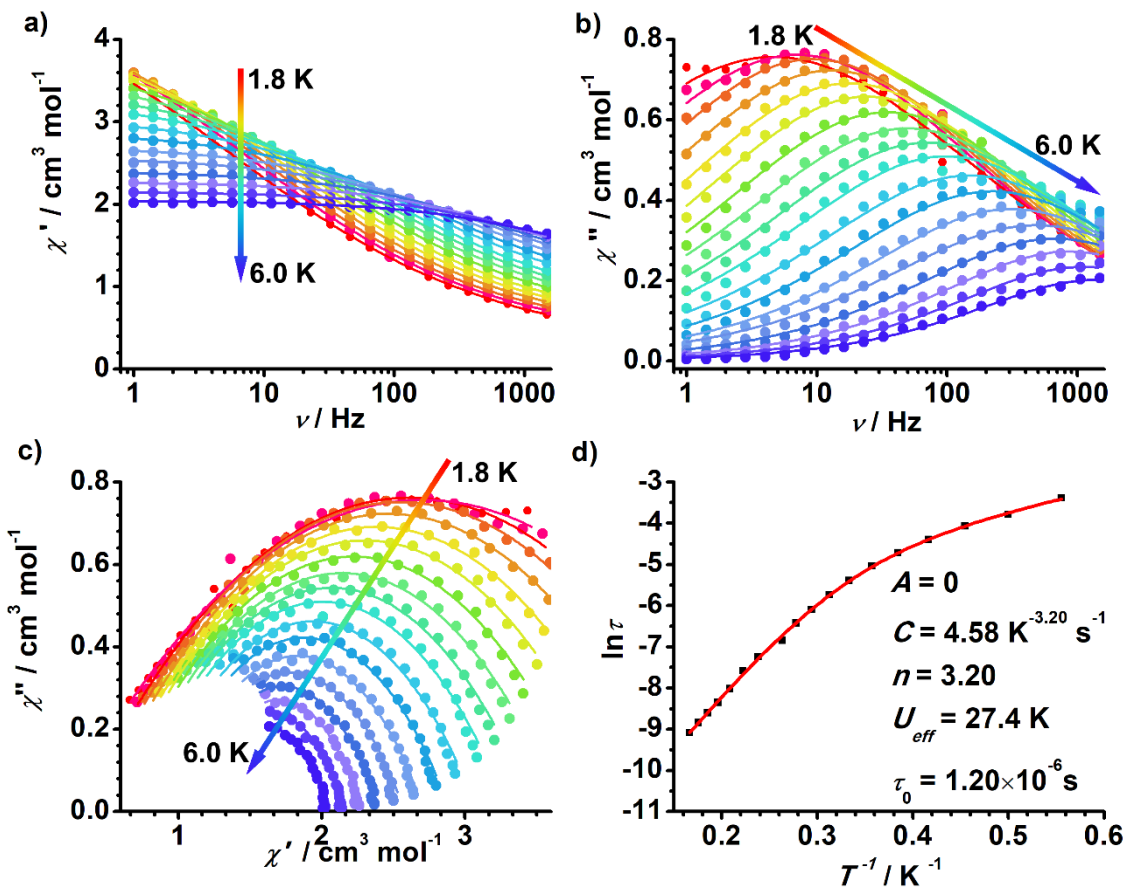


Figure S27. Frequency dependence of the in-phase (χ' , a) and out of phase (χ'' , b) ac susceptibilities, Cole-Cole plots (c) and corresponding plot of $\ln \tau$ vs. T^{-1} (d) for compound **2** measured in 1 kOe dc field. The solid line represents the best fitting.

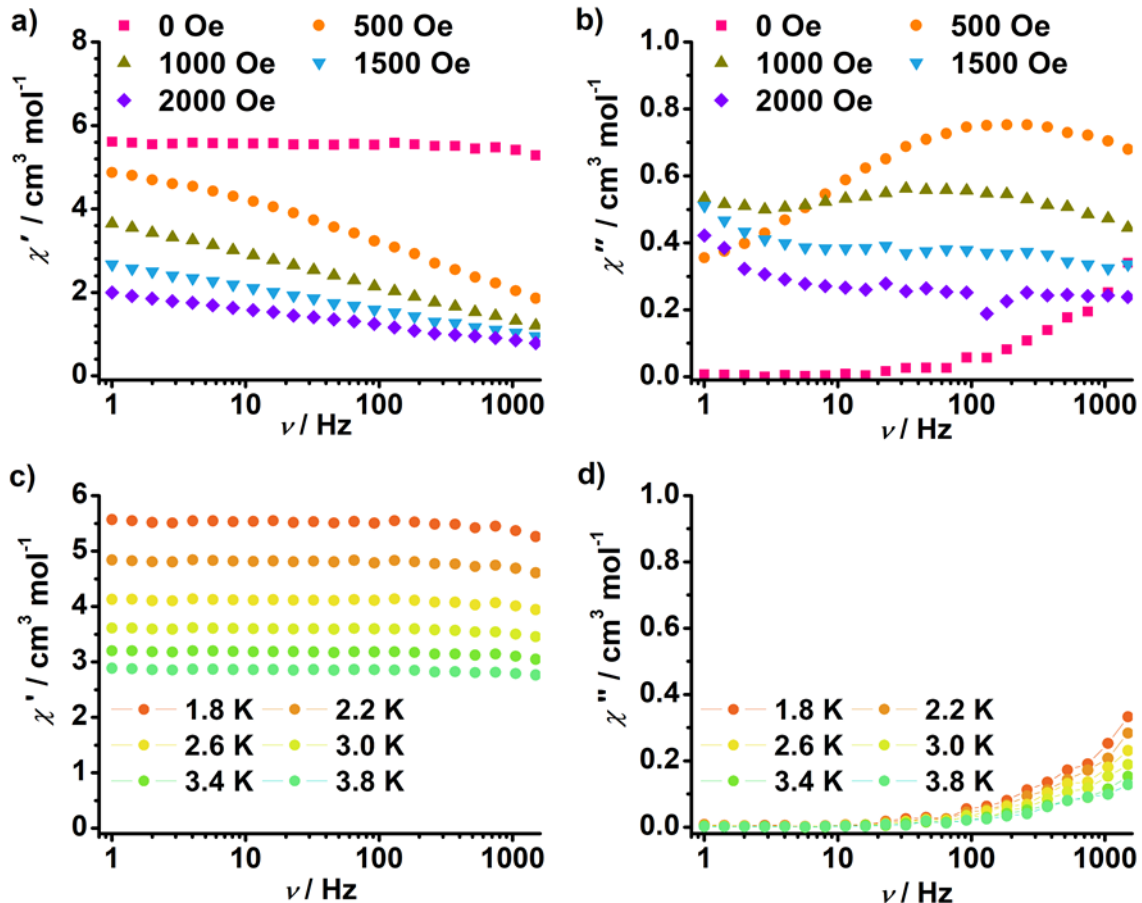


Figure S28. Frequency dependence of the in-phase (a) and out-of-phase (b) signals for ground **2** in the indicated dc fields at 1.8 K. Frequency dependence of the in-phase (c) and out-of-phase (d) signals for ground **2** under zero dc field.

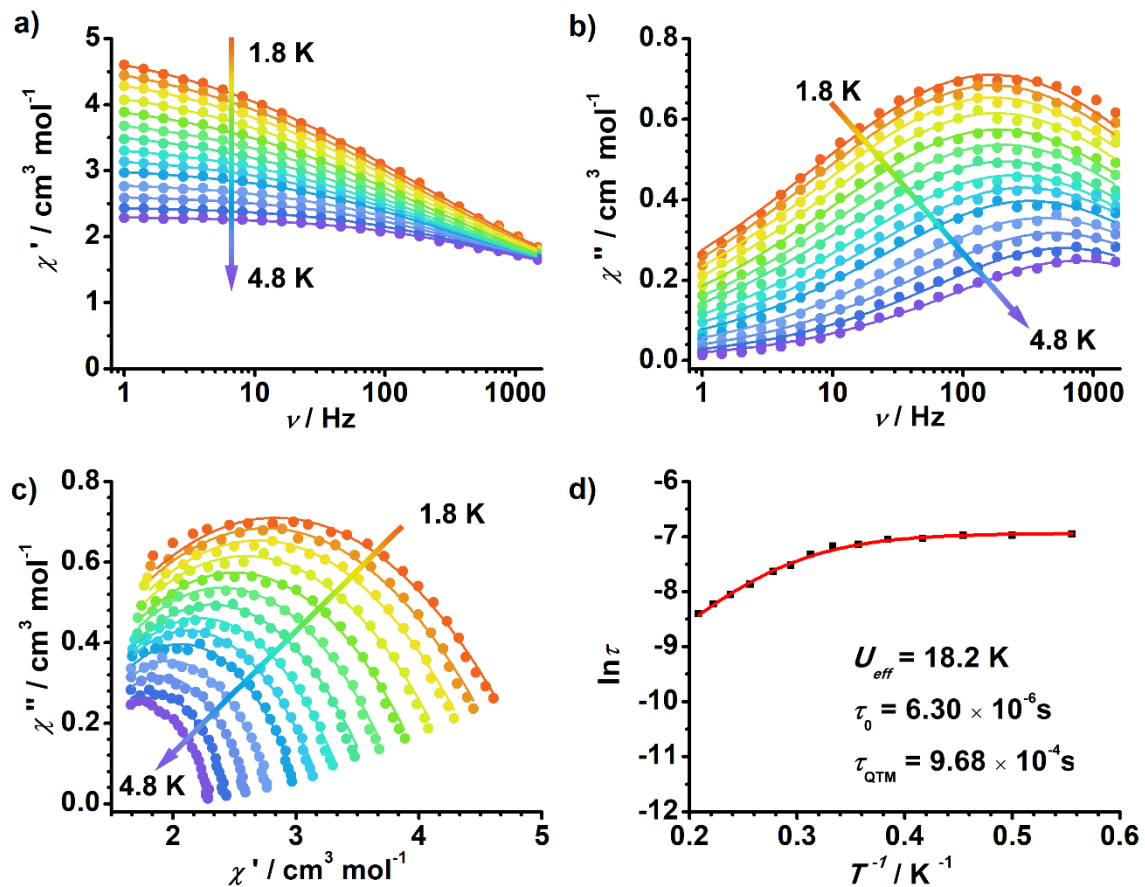


Figure S29. Frequency dependence of the in-phase (χ' , a) and out of phase (χ'' , b) ac susceptibilities, Cole-Cole plots (c) and corresponding plot of $\ln \tau$ vs. T^{-1} (d) for ground 2 measured at 0.5 bias kOe dc field. The solid line represents the best fitting.

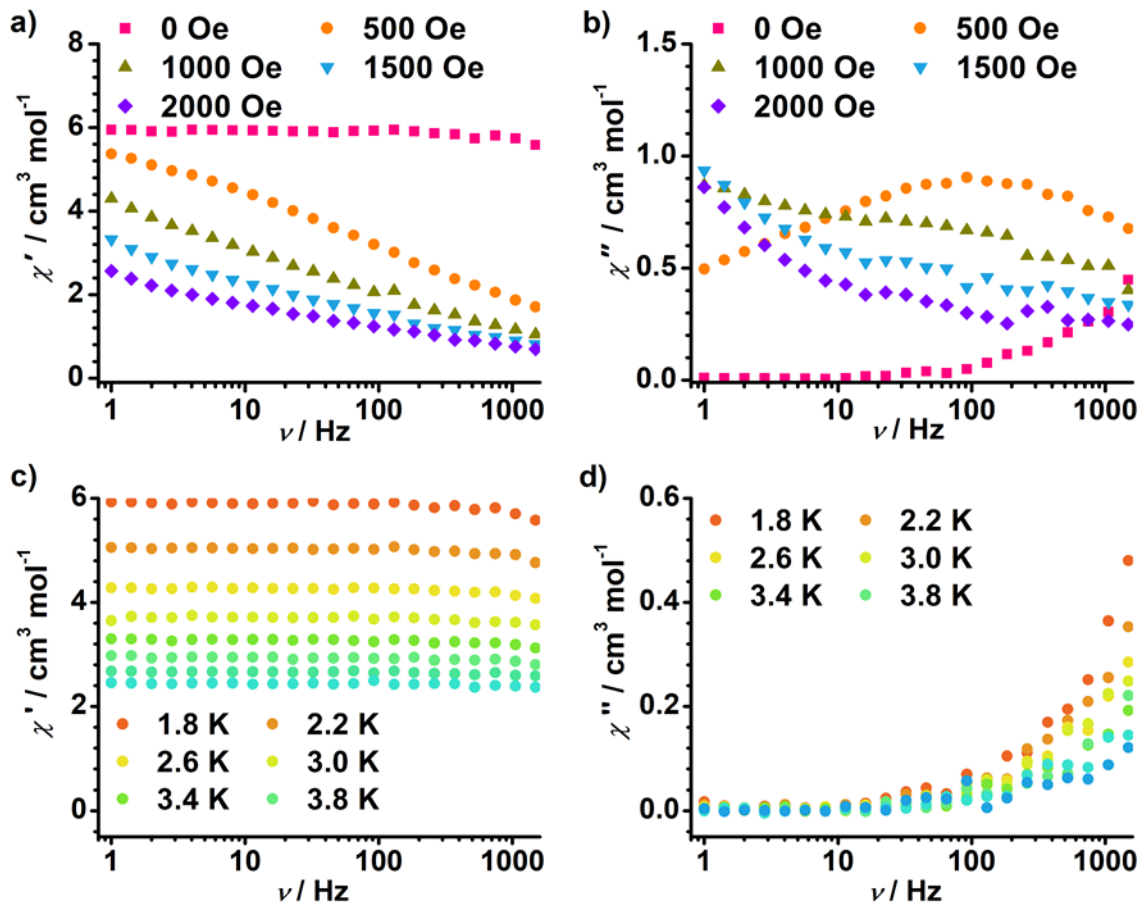


Figure S30. Frequency dependence of the in-phase (a) and out-of-phase (b) signals for ground and heated **2** in the indicated dc fields at 1.8 K. Frequency dependence of the in-phase (c) and out-of-phase (d) signals for ground and heated **2** under zero dc field.

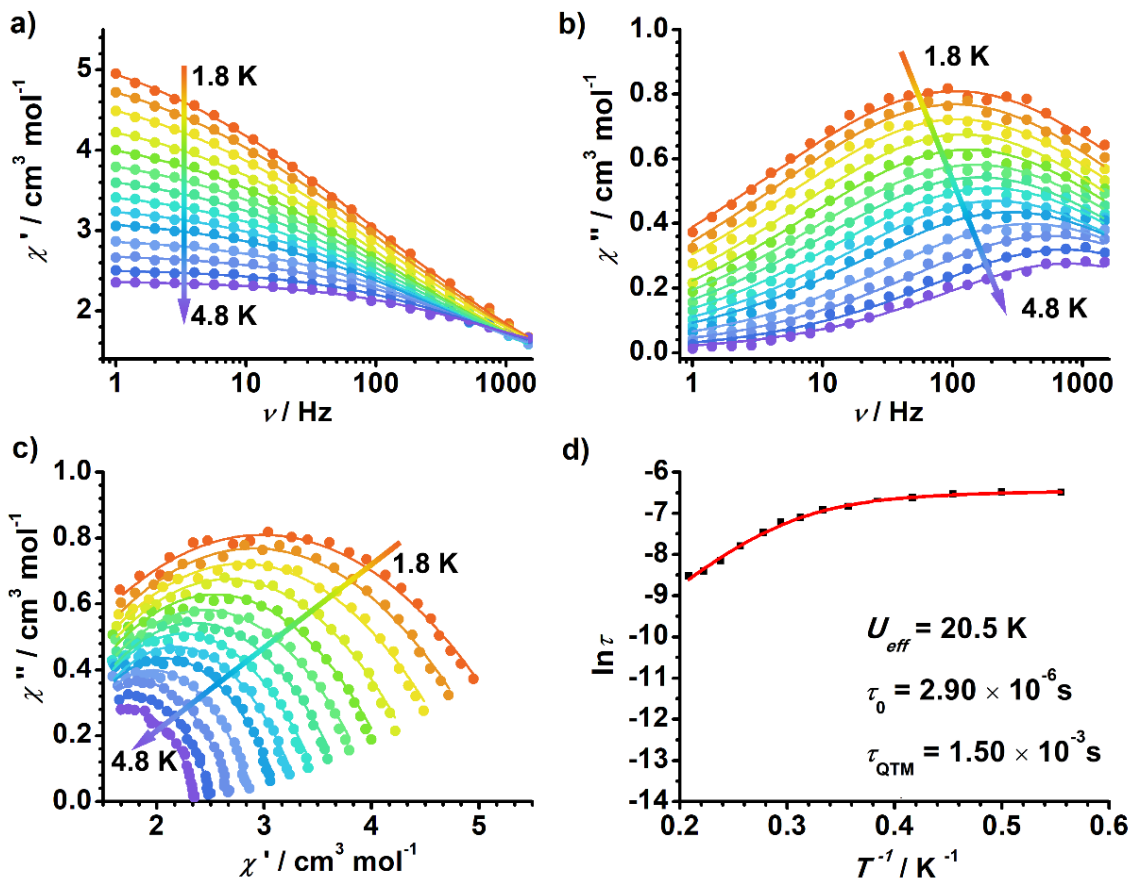


Figure S31. Frequency dependence of the in-phase (χ' , a) and out of phase (χ'' , b) ac susceptibilities, Cole-Cole plots (c) and corresponding plot of $\ln \tau$ vs. T^{-1} (d) for ground and heated **2** measured at 0.5 kOe dc field. The solid line represents the best fitting.